

# CoMFA, CoMSIA, and Molecular Hologram QSAR Studies of Novel Neuronal nAChRs Ligands-Open Ring Analogues of 3-Pyridyl Ether

Huabei Zhang,\* Hua Li, and Chunping Liu

Department of Chemistry, Beijing Normal University, 19# Street Xijiekou, Beijing, China, 100875

Received June 10, 2004

3-Pyridyl ethers are excellent nAChRs ligands, which show high subtype selectivity and binding affinity to  $\alpha 4\beta 2$  nAChR. Although the quantitative structure–activity relationship (QSAR) of nAChRs ligands has been widely investigated using various classes of compounds, the open ring analogues of 3-pyridyl ethers have been less involved in these studies due to the greater flexibility of this kind of molecule. In this study, two three-dimensional QSAR techniques and one two-dimensional QSAR technique were used to correlate the molecular structure with the biological activity of 64 analogues of 3-pyridyl ethers. Three different QSAR models were established. Their performances in the QSAR studies of open ring analogues of 3-pyridyl ethers were evaluated by the statistical values in the corresponding models. All models exhibited satisfactory predictive power. Of these models, the HQSAR behaved optimally in terms of the statistical values with  $q^2 = 0.845$ ,  $r^2 = 0.897$ . Finally, graphic interpretation of three different models provided coincident information about the interaction of the ligand–receptor complex and supplied useful guidelines for the synthesis of novel, potent ligands.

## INTRODUCTION

Neuronal nicotinic acetylcholine receptors (nAChRs) are subtypes of cholinergic receptor, which are pentameric ligand-gated channel and expressed as various combinations of  $\alpha$  and  $\beta$  subunits in the whole neural system. The predominant type in the mammalian brain is the  $\alpha 4\beta 2$  nAChR.<sup>1,2</sup> Over recent years, neuronal nAChRs have received great interest due to their intimate involvement in various important CNS functions and pathological states.<sup>3–6</sup> The pharmaceutical potential of ligands with high receptor subtype-selectivity and high receptor binding affinity in related disorders and states has been widely recognized, which spurred a great deal of effort to develop potent nAChRs ligands.

However, the therapeutic application of the prototype agonist of nAChRs is limited due to the untold side effects, such as nicotinic, epibatidine and anatoxin-a, and so on. To search nAChRs ligands with better ratios of pharmacological to toxicological activities, a large variety of compounds have been synthesized and evaluated.<sup>7,8</sup> The newly developed 3-pyridyl ether analogue displayed promising therapeutic potent for its excellent properties on  $\alpha 4\beta 2$  receptor with a high pM binding affinity coefficient and a much higher subtype-selectivity than the most potent epibatidine.<sup>7,8</sup> Based on the first 3-pyridyl ether compound A-84543<sup>9</sup> (Table 1), new compounds have been explored by structural alteration.<sup>10–16</sup> The recently open ring analogues of A-84543 were synthesized by Lin et al.,<sup>17</sup> of which some maintained or even improved the receptor affinity as that of the lead compound. Using QSAR as a tool to predict potent molecules is still a most attractive approach. However, due to the

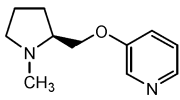
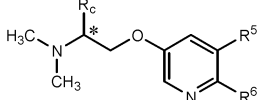
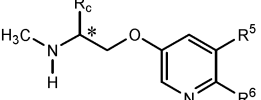
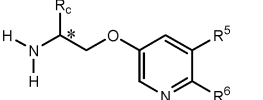
relative larger number of flexible bonds in the pyridyl ether compounds, especially in the open ring compounds, a few of these compounds had been investigated as a QSAR study.

As for nicotinic ligands, some QSAR models and pharmacophore models have been proposed.<sup>18–22</sup> Moreover, based on the available crystal structure of AChBP (acetylcholine binding protein), the high homologous protein of nAChR extracellular domain,<sup>23,24</sup> some structure-based ligand design has also been performed.<sup>25–28</sup> Unfortunately, the lack of an atomic level structural detail made the crystal structure inefficient for reliable drug design. For diverse congeneric compounds, whether the way of ligands interacted with the receptors is homogeneous or heterogeneous is still being debated. A QSAR study of novel ligands will help to understand the nature of the interaction between the nicotinic ligand and nAChRs. In this study, we used three different QSAR techniques, two three-dimensional QSAR techniques (CoMFA method and CoMSIA method) and one two-dimensional QSAR technique (molecular hologram QSAR methods, HQSAR) to explore the QSAR of these open ring analogues in order to derive some useful information to guide the synthesis of novel potent ligands and to complement the current accepted pharmacophore models.

CoMFA and CoMSIA have become popular in QSAR studies, while the molecular hologram QSAR (HQSAR) is a new development method,<sup>29</sup> which has already been successfully applied to different classes of compounds.<sup>30–32</sup> The CoMFA and CoMSIA methods are potential based methods, which correlate the biological data with the fields properties generated around the aligned molecules using certain probes at a space grid. They can give information of interaction between ligand and putative receptors. In contrast, HQSAR relates the biological activities with 2D molecular structural compositions, described in terms of substructural

\* Corresponding author phone: +86-10-58805194; fax: +86-10-58800567; e-mail: hbzhang@bnu.edu.cn.

**Table 1.** Experiment, CoMFA, CoMSIA, HQSAR-Predicted  $pK_i$  Values of Training and Test Set Molecules

<div style="display: flex; justify-content: space-around; align-items: center;"> <div style="text-align: center;">  <p>A-84543</p> </div> <div style="text-align: center;">  <p>Series a</p> </div> <div style="text-align: center;">  <p>Series b</p> </div> <div style="text-align: center;">  <p>Series c</p> </div> </div>									
name	chirality	R <sub>c</sub>	R <sup>5</sup>	R <sup>6</sup>	K <sub>i</sub>	pK <sub>i</sub>	CoMFA	CoMSIA	HQSAR
Training Set									
3a		H	H	H	32.6	7.49	6.851	6.749	6.922
4a		H	Cl	H	74	7.13	6.92	6.927	7.006
6a		H	CF <sub>3</sub>	H	250	6.60	6.59	6.605	5.855
7a		H	NO <sub>2</sub>	H	260	6.59	5.749	6.373	6.445
8a		H	H	Me	140	6.85	7.465	7.362	6.961
10a		H	H	Cl	79	7.10	7.445	7.554	7.611
11a	R	H	Cl	Cl	16	7.80	7.527	7.743	7.779
12a	S	H	Br	Cl	7.1	8.15	7.773	7.908	7.796
14a	S	Me	H	Cl	42	7.38	7.163	7.656	7.607
15a	R	Me	H	F	70	7.16	7.176	7.208	7.571
16a	S	Me	H	F	100	7.00	6.935	7.334	6.983
17a	R	Me	Br	Cl	12	7.92	7.934	7.925	8.381
18a	S	Me	Br	Cl	31	7.51	7.347	8.042	7.792
20a	S	Me	Me	Cl	9.6	8.02	7.735	8.09	7.954
21a	R	Me	4-py-CH=CH	Cl	0.1	10.00	10.088	10.105	9.934
22a	S	Me	4-py-CH=CH	Cl	0.37	9.43	9.214	9.698	9.345
24a	S	CH <sub>2</sub> Ph	4-py-CH=CH	Cl	4.6	8.34	8.554	8.156	8.097
25a	S	CH <sub>2</sub> Ph	Br	Cl	320	6.49	6.861	6.444	6.544
27a	S	H	H	H	17	7.77	7.281	6.949	7.119
28a	S	H	Cl	H	37	7.43	7.318	7.133	7.203
30b		H	NO <sub>2</sub>	H	560	6.25	6.232	6.554	6.642
31b		H	CF <sub>3</sub>	H	1500	5.82	6.909	6.802	6.051
31'b		H	H	Me	43	7.37	7.854	7.562	7.158
32b		H	H	OMe	620	6.21	6.962	6.719	6.674
33b		H	H	Cl	22	7.66	7.82	7.755	7.808
34b		H	Cl	Cl	13	7.89	7.903	7.95	7.976
36b	R	Me	H	Cl	5.9	8.23	7.76	7.798	8.346
37b	S	Me	H	Cl	41.0	7.39	7.665	7.71	7.948
38b	R	Me	H	F	11	7.96	7.572	7.486	7.722
39b	S	Me	H	F	69	7.16	7.248	7.352	7.324
40b	R	Me	Br	Cl	1.5	8.82	7.951	8.195	8.531
41b	S	Me	Br	Cl	11.0	7.96	7.996	8.082	8.133
43b	S	Me	Me	Cl	5.5	8.26	8.216	8.162	8.295
44b	R	Me	4-py-CH=CH	Cl	0.077	10.14	10.001	9.895	10.085
45b	S	CH <sub>2</sub> Ph	4-py-CH=CH	Cl	2.6	8.59	8.318	8.672	8.445
47b	S	CH <sub>2</sub> Ph	H	H	690	6.16	6.855	6.037	6.017
48b	S	Et	H	F	220	6.66	7.126	7.215	7.272
49c		H	Cl	H	140	6.85	7.497	7.608	7.284
50c	R	Me	H	Cl	5.3	8.28	8.148	8.214	8.344
51c	S	Me	H	Cl	4.5	8.35	8.181	8.091	8.102
53c	S	Me	H	F	8.7	8.06	7.779	7.734	7.478
54c	R	Me	Br	Cl	1.5	8.82	8.501	8.593	8.529
55c	S	Me	Br	Cl	1.5	8.82	8.526	8.451	8.287
56c	R	Me	Me	Cl	0.98	9.01	8.743	8.693	8.691
58c	R	Me	4-py-CH=CH	Cl	0.081	10.09	10.162	10.027	10.083
59c	S	Me	4-py-CH=CH	Cl	0.076	10.12	10.363	10.425	9.84
61c	S	CH <sub>2</sub> Ph	4-py-CH=CH	Cl	9.9	8.00	8.805	7.703	8.62
62c	S	Et	Br	Cl	15	7.82	7.582	7.99	8.232
63c	S	CH <sub>2</sub> Ph	Br	Cl	100	7.00	7.34	6.743	7.067
64c	S	Et	H	F	39	7.41	7.376	7.134	7.423
Test Set									
5a <sup>c</sup>		H	Br	H	50	7.30	7.143	8.214	8.344
9a <sup>c</sup>		H	H	OMe	406	6.39	7.759	7.177	6.478
13a <sup>c</sup>	R	Me	H	Cl	42	7.38	7.58	7.566	8.195
19a <sup>c</sup>	R	Me	Me	Cl	7.2	8.14	8.133	8.013	8.543
23a <sup>c</sup>	R	Et	4-py-CH=CH	Cl	3.6	8.44	9.953	9.627	9.275
26a <sup>c</sup>	S	CH <sub>2</sub> CH <sub>2</sub> Cl	CF <sub>3</sub>	H	5.5	8.26	6.669	6.725	5.881
29b <sup>c</sup>		H	NH <sub>2</sub>	H	27	7.57	7.859	7.44	7.248
35b <sup>c</sup>		H	Br	Cl	14.3	7.84	8.162	8.119	7.993
42b <sup>c</sup>	R	Me	Me	Cl	0.57	9.24	8.33	8.235	8.694
46b <sup>c</sup>	S	CH <sub>2</sub> Ph	Br	Cl	85	7.07	7.784	7.217	6.892
52c <sup>c</sup>	R	Me	H	F	6.6	8.18	7.751	7.862	7.72
57c <sup>c</sup>	S	Me	Me	Cl	0.52	9.28	8.724	8.54	8.449
60c <sup>c</sup>	S	Et	4-py-CH=CH	Cl	0.18	9.74	10.16	10.076	9.785
65c <sup>c</sup>	S	Et	H	Cl	15.0	7.82	7.474	7.55	8.047
							$r^2_{\text{pred}}^a$	0.374	0.399
							$r^2_{\text{pred}}^b$	0.504	0.663

<sup>a</sup> Square of correlated coefficient of predicted value of all molecules in test set. <sup>b</sup> Square of correlated coefficient of predicted value of molecules in test set with compound 26 removed. <sup>c</sup> Molecules were selected as test sets.

fragments. The most attractive advantage of HQSAR is its relative independence of the 3D molecular structure, which is not explicitly encoded in the HQSAR descriptor. Moreover, HQSAR can suggest intuitionistic guidelines for structural modification for novel compound design. Joint application of 3D QSAR with the 2D fingerprint properties could give a more reliable and efficient route to the synthesis of ligands with high affinity and specificity.

## MATERIAL AND METHODS

**Data Set.** A total 64 compounds were taken from the published work of Nan-Horng Lin et al.<sup>17</sup> Because the differences in molecular structural properties and biological activities of ligands were primary considerations in a QSAR study, the use of charged or uncharged molecules in modeling currently is still being debated.<sup>33</sup> The study of Gohlke et al.<sup>34</sup> suggested that QSAR on nAChR ligands in the natural form resulted in better statistics than that in the protonated form. Our previous study<sup>35</sup> also drew the same conclusion. Thus in this study we used unprotonated molecules to perform the QSAR study. The structures of these compounds and their biological data were given in Table 1. The binding affinity  $pK_i$  ( $-\log K_i$ ) values for  $\alpha 4\beta 2$  nAChR were used as dependent variables in the CoMFA, CoMSIA and HQSAR analyses. The investigated compounds were homogeneous, and we could reasonably think that they bound to the receptor in the same fashion. To obtain reliable results, the total set was divided into a training set of 50 compounds and a test set of 14 compounds. The biological data of the training set had an even distribution and spread over a range of five logarithmic units. The test set was selected to be similar in chemical classes and a range of  $pK_i$  values to that of the training set.

**Molecular Modeling.** In the development of 3D-QSAR models, the choice of analogues conformation was important in providing a realistic pharmacophore. Unfortunately, so far no reliable ligand–receptor complex has been solved at the atomic levels. Moreover, since the studied compounds are very flexible, the ascertainment of the active conformation is difficult. The active conformation of each analogue had to be approximated. In this study, a minimum-energy structure optimized by the AM1 semiempirical protocol was used as an active conformation. Possibly, the conformation (calculated in a vacuum) may differ widely from the biologically active conformation. A MM+ random conformation search protocol and AM1 semiempirical protocol in Hyperchem 7.0 software package<sup>36</sup> were used to determine the minimum energy structure. All the molecules were generated and optimized in the Hyperchem 7.0 software package. The structure was first optimized using molecular mechanics with an MM+ force field. Then a conformation search of the preliminary optimized structures was performed using the Monte Carlo method and MM+ force-field parameters in Hyperchem 7.0 software package, which found the lowest-energy conformations of a molecule by varying specified dihedral angles. The 25 lowest-energy conformations obtained from the conformation search were further optimized using the semiempirical method AM1 in order to obtain global minimum energy conformation. The final global minimum energy conformation with the AM1 partial charge was then saved into Sybyl molecular format (mol2

file). Sometimes the atom type in mol2 file saved from the Hyperchem software package could not be recognized by Sybyl software, and then a modified protocol with only atom types changed in the Sybyl software package was used for atom type alteration. The lowest-energy conformation with the AM1 partial charge was used for CoMFA, CoMSIA and HQSAR modeling using the Sybyl 6.91 software package.<sup>37</sup>

**Database Alignment.** Compound 56 was chosen as the alignment template because of its higher affinity for  $\alpha 4\beta 2$  nAChR and its representative structure of these molecules. To the best of our knowledge, the definitive pharmacophore model is still unclear. The current popularly accepted pharmacophore elements of the nicotinic ligand are as follows: the pyridyl nitrogen, the pyridyl centroid, the pyrrolidinyl nitrogen and the pyrrolidinyl centroid.<sup>22</sup> For ether compounds, the ether oxygen atom also contributed a lot to the affinity.<sup>38</sup> To obtain a more compact alignment, we used the following atoms as the reference atoms for alignment: (i) the aromatic pyridyl ring, (ii) the ether oxygen, and (iii) the  $sp^3$ -hybridized nitrogen atom of the chain. The molecular alignment used for the studies was obtained by means of the SYBYL 6.91 database alignment protocol.

## CALCULATION OF QSAR DESCRIPTORS

**CoMFA and CoMSIA.** For the CoMFA calculation, the alignment molecules were placed in a 3D cubic lattice with 2 Å spacing. The default  $sp^3$  carbon atom with a +1 charge was selected as the probe atom for the calculations of the steric (Lennard-Jones 6–12 potential) and electrostatic fields (Coulombic potential) around the aligned molecules with a distance-dependent dielectric constant at all lattice points. The column filtering was set to 1.0 kcal/mol. Values of steric and electrostatic energies were truncated at 30 kcal/mol.

The same grid constructed for the CoMFA field calculation was used for the CoMSIA field calculation.<sup>39,40</sup> Five physicochemical properties (steric, electrostatic, hydrophobic, hydrogen bond donor, and hydrogen bond acceptor) were evaluated using the probe atom. A probe atom  $sp^3$  carbon with a charge of +1, hydrophobicity of +1, and H-bond donor and acceptor property of +1 was placed at every grid point to measure the electrostatic, steric, hydrophobic, and H-bond donor or acceptor field. Different from the CoMFA, a Gaussian type distance dependence of physicochemical properties was used in CoMSIA. Thus no singularities occurred and no arbitrary cutoffs were required. The default value of 0.3 was used as the attenuation factor (R).

**HQSAR.** In HQSAR, a molecule is described as a unique string of numbers or “bins” (molecular hologram). The bins represent all of the unique fragments included within a particular molecule and are assigned by a cyclic redundancy check (CRC) algorithm. All linear, branched and overlapping structure fragments were used to generate HQSAR descriptors. The structure fragments from each original molecule consisted of a user defined minimum and a maximum number of atoms, which are fragment size parameters. The information in each fragment is defined by fragment distinction parameters, including atoms (A), bonds (B), connections (Con), hydrogen (H), chirality (Ch) and H donor or acceptor (DA). The generated fragments were then hashed into a fixed length array to produce a molecular hologram. The fixed length was defined as hologram length parameters. The

**Table 2.** Summary of Results from the CoMFA, CoMSIA Analyses<sup>a</sup>

	CoMFA SE	SE	CoMSIA SE&H&DA	SE&H
Statistical Result				
$q^2$	<b>0.652</b>	0.535	0.516	<b>0.582</b>
$r^2$	<b>0.847</b>	0.769	0.749	<b>0.876</b>
SD	<b>0.418</b>	0.514	0.535	<b>0.380</b>
F	<b>130.392</b>	78.279	70.276	<b>108.746</b>
components	<b>2</b>	2	2	<b>3</b>
Fraction (%)				
steric	<b>0.655</b>	0.319	0.165	<b>0.218</b>
electric	<b>0.345</b>	0.681	0.223	<b>0.446</b>
hydrophobic			0.243	<b>0.336</b>
donor			0.155	
acceptor			0.215	

<sup>a</sup> SE: steric and electrostatic fields; DA: hydrogen donor and hydrogen acceptor fields; H: hydrophobic field;  $q^2$ : square of cross-validated correlated coefficient from L–O–O analysis;  $r^2$ : square of non-cross-validated correlated coefficient; SD: standard error of prediction. F: value of F-test which denotes ratio of  $r^2$  explained to unexplained)  $r^2/(1 - r^2)$ .

HQSAR module provides 12 default hologram lengths (53, 59, 61, 71, 83, 97, 151, 199, 257, 307, 353, and 401), which are prime numbers, to minimize the possibility of fragment collision. The particular nature of substructure fragments generated by HQSAR and, consequently, the information contained in the resultant molecular holograms was altered by adjusting these parameters.

**PLS Analyses.** CoMFA, CoMSIA, and HQSAR models have been derived from a training set of 50 nAChRs ligands. The method of PLS regression was used to correlate variations in the biological activities with variations in the respective descriptors. Cross-validation was undertaken using the L–O–O procedure. First, the optimum number of components (ONC) was obtained by performing L–O–O analysis with SAMPLS.<sup>41</sup> The optimal number of components was determined in such a way that each additional component should increase the  $q^2$  by at least 5% to prevent training set overfit.<sup>34</sup> With the optimum number of components, a non-cross-validation was performed to establish the model for predicting the affinities of the compound in the training set and the test set.

## RESULTS AND DISCUSSION

**CoMFA and CoMSIA Models.** Several statistical significant models were obtained (Table 2). Final models were selected based on the better values of  $q^2$  (square of the cross-validated correlated coefficient), predictive  $r^2$  (square of the non-cross-validated correlated coefficient) and predictive standard error (all of these are boldfaced in Table 2).

A CoMFA model containing steric and electrostatic fields was built up. For the CoMSIA methods, more fields were introduced to compare similarity of the fields of the aligned molecules. These included steric, electrostatic, hydrophobic, hydrogen donor and hydrogen acceptor fields. So it could give more information of specific properties of interactions between the ligands and the receptor.

The cross-validation  $q^2$  of the CoMFA model was 0.652, with two components. The non-cross-validation  $r^2$  was 0.847, with the standard error of 0.418. Compared with the CoMFA model, the CoMSIA models were slightly inferior in the

**Table 3.** Influence of Various Fragment Type Parameters for the 50 Compound Database Using Fragment Size Default (4–7)

stastical parameters	$q^2$	$r^2$	$S^a$	best length	ONC
A+B	0.824	0.925	0.469	83	6
A+B+Con	0.832	0.932	0.469	53	8
A+B+H	0.818	0.910	0.476	151	6
A+B+Ch	0.841	0.929	0.440	61	5
<b>A+B+Con+Ch</b>	<b>0.845</b>	<b>0.897</b>	<b>0.425</b>	<b>61</b>	<b>3</b>
A+B+Con+H	0.831	0.928	0.464	257	7
A+B+H+Ch	0.836	0.943	0.463	83	8

**Table 4.** Influence of Various Fragment Size Parameters for the 50 Compound Database Using Atom/Bond/Connectivity/Chirality as Fragment Type

fragment length	$q^2$	$r^2$	S	best length	ONC
2–5	0.832	0.933	0.470	59	8
3–6	0.837	0.945	0.462	71	8
5–8	0.847	0.939	0.436	61	6
6–9	0.852	0.953	0.441	53	8
7–10	0.855	0.961	0.436	199	8
3–10	0.861	0.956	0.436	53	8

ability to predict with cross-validation  $q^2$  values around 0.55. Of the three CoMSIA models, the model comprised of steric, electrostatic and hydrophobic fields exhibited the highest cross-validation  $q^2$  and was selected as the final CoMSIA model for prediction. The non-cross-validation  $r^2$  was 0.876, with three components and a standard error value of 0.380.

**HQSAR Models.** The performance of the HQSAR models was affected by three parameters—the fragments size, the hologram length and the fragments type (fragment distinction). The HQSAR model was first generated with a default fragment size (4–7) combined with various fragment types and various hologram lengths. Table 3 summarizes the results for the different fragment types and hologram lengths. The best model was obtained using a hologram length of 61 and **A+B+Con+Ch** as the fragment type ( $q^2 = 0.897$ ,  $S = 0.845$ , ONC = 3). The information from fragment types such as Atoms, Bonds, Connection and Chirality made an important contribution to the biological activity. With the best fragment type parameters, PLS analyses were performed to investigate if different fragment lengths could improve the statistical parameters. The HQSAR results from the different fragment sizes are summarized in Table 4. Larger fragment size was favored for improving the statistic data. However, the increment was not significant, only 0.23 when the fragment size changed from 2–5 to 7–10. To avoid over interpretation, we chose a model with a higher  $q^2$  and a smaller number of components as the final HQSAR model. This HQSAR model was built using Atom/Bond/Connectivity/Chirality as the Fragment Type and 4–7 as the fragment size, with a hologram length of 61 ( $q^2 = 0.845$ ,  $r^2 = 0.897$ , ONC = 3, Table 5).

## VALIDATION AND COMPARISON OF THE QSAR MODELS

In addition to evaluation by the training set, the predictive power of the QSAR model should be further validated by performing a test set prediction. The selected three models (boldfaced in Table 2 and Table 5) were used to predict the binding affinity for the training set and the test set. The predicted versus the measured pKi values for the training and the test sets were listed in Table 1 and depicted



**Table 5.** Statistical Results of HQSAR Analysis<sup>a</sup>

fragment length (fragment type)	$q^2$	$r^2$	SD	F	ONC
4–7(A+B+Con+Ch)	<b>0.845</b>	<b>0.897</b>	<b>0.346</b>	<b>133.915</b>	<b>3</b>

<sup>a</sup> A: atom, B: bond, Con: connection, Ch: chirality, H, hydrogen;  $q^2$ : square of cross-validated correlated coefficient from L–O–O analysis;  $r^2$ : square of non-cross-validated correlated coefficient; S: standard deviation of  $q^2$ ; SD: standard error of prediction. F: value of F-test which denotes ratio of  $r^2$  explained to unexplained ( $r^2/(1 - r^2)$ ).

graphically in Figure 1 for the CoMFA, CoMSIA, and HQSAR models, respectively. All three models showed a high degree of predictive power (with the residues generally less than one logarithmic unit).

As shown in the plots of predicted versus measured p*K*<sub>i</sub> values, three models all failed to predict compound 26, especially the HQSAR model which showed a large predictive residue of –2.38 for compound 26. The bad prediction of compound 26 might ascribe to its unique R<sub>c</sub> group of CH<sub>2</sub>–CH<sub>2</sub>Cl substituted on the chiral carbon atom on the long chain moiety in the whole database. For the whole test set including compound 26, the CoMSIA model was most predictive with the highest  $r^2_{\text{pre}}$  value of 0.452 (Table 1), where CoMFA and CoMSIA showed similar inferior predictive power in terms of the  $r^2_{\text{pre}}$  values of 0.374 and 0.399, respectively. However, when compound 26 was excluded, the HQSAR model showed the highest predictive power with a pretty  $r^2_{\text{pre}}$  value of 0.663. It seemed that the substructure-based QSAR technique was not particularly ideal for molecules possessing substructures not presented in the training set, whereas the potential field-based technique CoMSIA seemed better suited for extrapolations to bioisosteric substructures in molecules.

More rigorous statistical testing was performed by group cross-validation, taking 8 compounds out of the whole database on five occasions. The average  $q^2$  values (N-fold) and standard deviations obtained in the group cross-validation were presented in Table 6. The average of  $q^2_{\text{LNO}}$  was in the similar range as that of the selected models, 0.628 for CoMFA, 0.525 for CoMSIA and 0.725 for the HQSAR model, respectively. The standard deviations (SD) in the  $q^2_{\text{LNO}}$  values from the group cross-validation results were minimal (0.009, 0.011, and 0.033 for the final CoMFA, CoMSIA and HQSAR models, respectively, all less than 4%). These results indicated that stability and robustness were characteristic of the CoMFA, CoMSIA and HQSAR models. The SD of  $q^2_{\text{LNO}}$  from the HQSAR model was a little bigger than that from the CoMFA and CoMSIA models, which might own to the singularity of compound 26.

#### INTERPRETATIONS OF THE QSAR MODELS

To aid in visualization, the CoMFA and CoMSIA contour maps of the field contributions (“stdev\*coeff”) of different properties were illustrated in combination with the most potential compound—59 in the following figures (Figures 2–4). The HQSAR presentations of some molecules were shown in Figure 5. The combined application of the different approaches enabled one to obtain a consensus, that serves as an efficient tool for further synthesis work.

**CoMFA and CoMSIA QSAR Models.** As seen from the figures, the different physicochemical fields properties

contours were mainly distributed in the region around the sp<sup>3</sup>-hybridized nitrogen (localized in the inner side region relative to the plane consisting of the chiral carbon and the hydrogen attached to it) and near the region enclosed to the 5-,6-position of the pyridyl aromatic cycle, suggesting their importance in adjusting the affinity of the ligands.

An interesting phenomenon about the force fields distribution was observed around the sp<sup>3</sup>-hybridized N on the long chain. As seen from the figures, the contours of different fields properties only distributed in the inner side region where the sp<sup>3</sup>-hybridized nitrogen localized, while no contour was observed in the outer side region where the R<sub>c</sub>-group (refer to Table 1) localized. In the inner side region surrounding the sp<sup>3</sup>-hybridized nitrogen, there were yellow contours for the steric properties maps of CoMFA and CoMSIA (Figure 3), indicating that less steric bulk groups around the sp<sup>3</sup>-hybridized nitrogen would increase the affinity. For hydrophobic properties maps of the CoMSIA model (Figure 4), hydrophilic favorable white contours appeared in this area. As for the electrostatic properties, confused even ambivalent colored contours were shown in this region for the CoMFA and CoMSIA models (Figure 2). As it was known, the CoMSIA method was less alignment-sensitive and could provide more interpretable contours than that of the CoMFA method.<sup>42</sup> In addition, the CoMSIA method was also presented to be more predictive than the CoMFA method in the test set prediction in the previous discussion. The blue contours shown on the sp<sup>3</sup>-hybridized nitrogen in the CoMSIA map should be more reasonable. The more positive charged nitrogen favored to increase affinity also agreed on the popularly accepted pharmacophore model,<sup>22</sup> where sp<sup>3</sup>-nitrogen interacted with the receptor through possible cation- $\pi$  interaction. In the outer side region around the R<sub>c</sub>-group, the variation of the fields did not show an apparent relationship to the affinity. Thus we inferred that the orientation of the sp<sup>3</sup>-N of the aminoethoxy caused rotation in some preferred direction to interact more fully with the receptor. A similar conclusion could also be derived from the crystal structure of AChBP, the highly homology of the extracellular domain of nAChR,<sup>23</sup> where the potential protonated nitrogen of the piperazine ring of HEPEs was closed to the rings of Trp143, indicating a possible cation- $\pi$  interaction between them. Thus, the region near the interaction direction would be sensitive to the variations of structural modification. An electron-withdrawing group with less steric bulk and lower lipophilicity in this region would be predicted to enhance the binding affinity. In other areas, this influence would be much less. Thus, fixing the orientation of the sp<sup>3</sup> N by introducing a rigid structure should favor enhanced affinity. This has been confirmed by the high affinities of various nAChR ligands with a nitric heterocycle. These include an azetidine ring, a pyrrolidine ring and a piperidine ring. Another QSAR study about the analogues of epibatidine also gave the same hypothesis.<sup>35</sup>

Another interesting region was the 5-position of the pyridyl ring. In electrostatic contour maps of CoMFA and CoMSIA (Figure 2), a large blue region appeared in the vicinity of the position 5 of the pyridyl ring, which indicated positive charged groups would benefit in enhancing the affinity. However, there were red contour distributions at distance areas near the pyridyl ring and the sp<sup>2</sup>-hybridized N of the 5-(4-py-CH=CH-) group. This has never been reported in

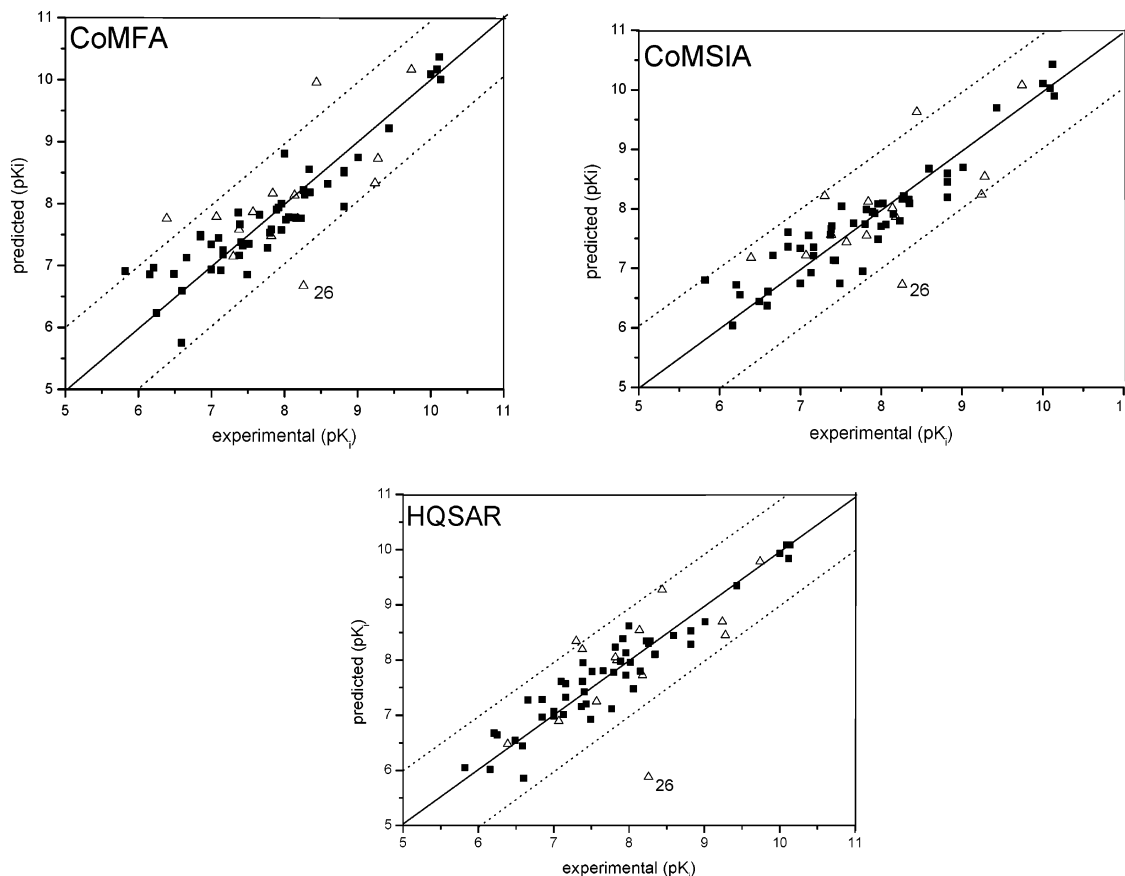


**Figure 1.** CoMFA, CoMSIA, and HQSAR predictions for the training (■) and test (Δ) sets. The fitted curves for CoMFA, CoMSIA, and HQSAR models are shown in three panels, respectively. The solid line is the ideal correlation line with slope values of 1, whereas the dotted lines indicate the  $\pm 1.0$  log point error margins.

**Table 6.** Leave-8-Out: Results of Group Cross-Validation Exercises

	FA_SE	SIA_SE	SIA_SE&DA&H	SIA_SE&H	HQSAR
run times	5	5	5	5	5
average $q^2$	0.628	0.525	0.550	0.525	0.725
SD $q^2$	0.009	0.011	0.024	0.016	0.033

previous QSAR studies, for which no compounds with comparable substitutes on this position were available at that time. Maybe the longer chains extended the substitute in a certain direction to another receptor binding pocket to make the electron of  $sp^2$ -N or pyridyl ring interact with the receptor through additional interactions, such as aromatic stacking with the benzene moiety of amino acids located within the nAChR binding domain. There was a large, sterically favorable region around the 5-position in CoMFA and CoMSIA steric fields contour maps (Figure 3). Increasing affinity could be predicted when steric bulky groups were introduced in this area. Small white unfavorable lipophilic areas also appeared near the 5-position (Figure 4), indicating that increasing lipophilicity would diminish the binding affinity. Thus, the 5-position might be localized in a relatively spacious pocket in the receptor binding domain. When the groups were not large enough, enhancing affinity could be prospected through increasing positive charge or steric bulk or hydrophilicity or a combination of them. Whereas when the groups were large enough to interact with residues on the wall of the receptor binding domain, enhanced affinity could be expected by increasing the negative charge of the group. It was interesting to note that a number of 3-pyridyl

ether analogues with large 5-aromatic ring substitutes have been reported to possess high affinity of pM magnitude,<sup>15,16</sup> which probably ascribed to an additional  $\pi$ - $\pi$  stacking interaction.

Near the region enclosed around the 6-position of the pyridyl ring, there were green steric contours, red electrostatic contours and yellow hydrophobic contours, representing those groups with steric bulk, rich electronic density and high lipophilicity. These favor increased affinity.

**Interpretation of HQSAR Models.** An attractive property of the HQSAR technique is that it provides straightforward clues about the individual atomic contributions to the biological activities through the use of different color codes. The colors at the red end (red, orange red and orange) of the spectrum reflect unfavorable contributions, while colors at the green end (yellow, green blue and green) reflect favorable contributions. Atoms with intermediate contributions are colored white. The cyan color code denotes the maximum common structure of the studied ligands.

The molecular hologram presentations for compounds based on the final HQSAR model were shown in Figure 5 for compounds 23, 24, 48, and 60, respectively. The conformation presented was the same as that used in the CoMFA and CoMSIA analyses. The different atomic contributions to the activity were summarized as follows:

For the group  $R_c$  which attached to the Chiral carbon on the long chain (refer to Table 1), yellow color presented on the methyl, red color on the benzene methyl. When the groups were ethyl, some interesting results were observed. As is shown in Figure 5, in the bimethylamine series (series

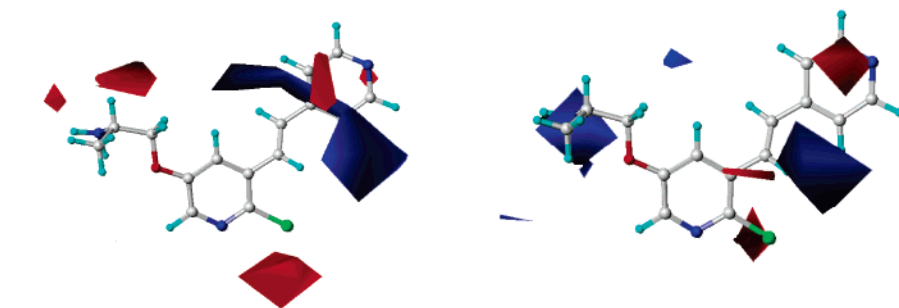


**Figure 2.** Contour plots of electrostatic field contributions ("stdev\*coeff") from the final models of CoMFA (left) and CoMSIA (right) in combination with compound 59. Blue contours (>80% contribution) and red (<20% contribution) contours correspond to regions where an increase in positive or negative charge, respectively, will enhance activity.

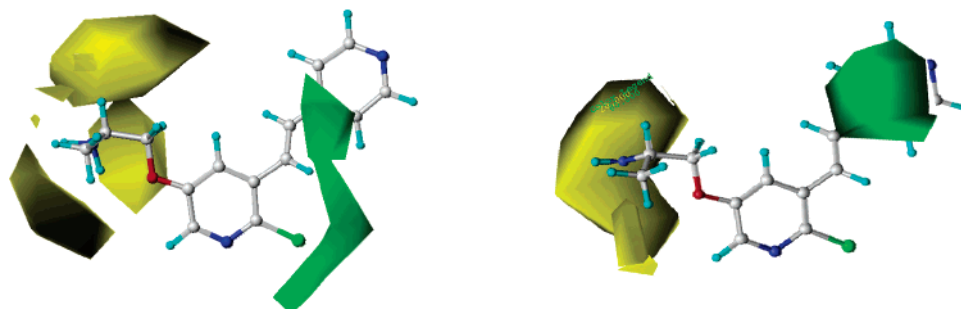


**Figure 3.** Contour plots of steric field contributions ("stdev\*coeff") from the final models of CoMFA (left) and CoMSIA (right) in combination with compound 59. Green contours (>80% contribution) indicate regions where an increase in steric bulk will enhance activity, and yellow contours (<20% contribution) indicate regions where an increase in steric bulk will reduce activity.

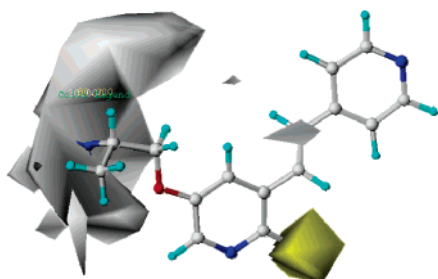


**Figure 4.** Contour plots of hydrophobic field contributions ("stdev\*coeff") from the final CoMSIA models in combination with compound 59. Yellow (>80% contribution) contours and white contours (<20% contribution) show regions where an increase in lipophilicity or hydrophilicity, respectively, will enhance activity.

a), the carbon atom of ethyl groups which attached to the Chiral carbon was colored in green, while it was colored in yellow in the methylamine series (series b) and white in the amine classes (series c). Thus we guessed that two interactions in these areas would probably contribute to the compound biological activity. One was the electrostatic interaction, and another was the van der Waals interaction. The former was the essential interaction and much larger than the latter. When there were two methyls on the  $sp^3$ -N, large steric bulk hindered the electrostatic interaction, while the volume of the two methyls and the ethyl substitutes favored the van der Waals interaction. In this situation, the ethyl became an important contributor to the ligand binding, thus green color code was shown on it in the HQSAR model. However, as the van der Waals interaction was far smaller than the electrostatic interaction, compounds of this class showed moderate but the lowest affinity in three classes. When there was no methyl on the  $sp^3$  N, no spacious hindrance existed for the electrostatic interaction, the electrostatic interaction completely become the primary contribu-

tion, then the van der Waals interaction show nearly little contribution and was shown in white in the HQSAR model. As for the single methylated ligands, both interactions contributed to increased affinity. The color code on the ethyl correspondingly was yellow, which was between that of the two formers. The study of Lucio Toma et al.<sup>43</sup> also pointed out that this van der Waals interaction could play a special role in enhancing the binding affinity of the nAChRs ligand. However, as it was described in the HQSAR model, the chirality of group  $R_c$  is one of the most contribution fragment types, the methylamino with R chirality ligands show higher affinity. In conclusion, a suitable volume of  $R_c$  group with a suitable orientation would improve the affinity, which coincided with the analyses of CoMFA and CoMSIA.

As to the 5-position, requirements here were more complicated because the substitutes varied considerably. When small groups were introduced to the 5-position, the yellow color occurred at the methyl groups, while the orange-red color occurred at nityl, the red color at trifluorid methyl, and the white color was presented at H, Cl and Br. This suggested that stronger electron withdrawing groups would impair the activity, and moderate volume groups were tolerated. However, when larger substitutes, such as 2-pyridyl-4-l-ethyl or 2-pyridyl-4-l-vinyl with rich electronic density, were presented, the color coded yellow to green suggested that these groups were favorable for affinity. These results coincided with the above CoMFA and CoMSIA models.

For the position 6- of the pyridyl ring, all the investigated groups generally showed a white color, such as H, F and  $CH_3$ , while the Cl atom coded as green, which indicated the Cl atom at this position would benefit to the activity. The Cl atom possibly fitted to the need of steric bulk and electronic density in this position just as what described in the CoMFA and CoMSIA models.



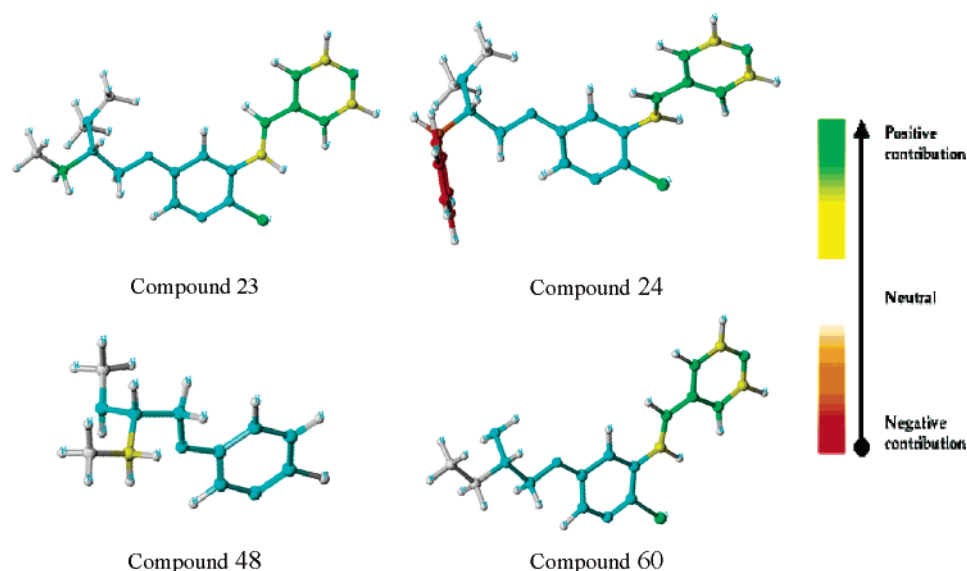


**Figure 5.** HQSAR presentations of compounds 23, 24, 48, and 60, respectively.

### CONCLUSION

Three different techniques have been used to generate QSAR models for a series of pyridyl ether analogues. The performances of these models were compared using several statistical measures, including  $r^2$ ,  $q^2$ , and the predictive standard errors. The obtained models were satisfied based on both statistical significance and predictive ability. Information derived from these models was generally in agreement with each other, suggesting that these models were robust enough for predicting novel ligands.

Of the three different models, the HQSAR model appeared to be the most predictive, with  $q^2$  values of 0.845 and the least predictive residues for almost all of the molecules except for the unique  $R_c$  substitute compound 26. It seemed that the substructure-based techniques were more suitable to similar structural analogues than the diversified compounds, for later the potential based CoMSIA technique was more robust.

The interpretation of the QSAR models also highlighted some specific properties of interaction between the series of ligands and the receptor. First, the proposed pharmacophore elements of the series of ligands were largely in agreement with the currently pharmacophore models, that were the  $sp^3$ -hybridized N and the pyridyl ring. For the pyridyl ethers analogues, the ether oxygen atom was also important to the high affinity. The difference of the much flexible amine was that the series of ligands complied the orientation requirement of the  $sp^3$ -hybridized N through the rotation of the flexible bond. Thus, in the preferred direction of the  $sp^3$ -hybridized N, less steric bulk and less lipophilic substitute with negative charge were favorable to increasing the activity, while on the other direction, suitable steric bulk were tolerated as it described in HQSAR presentations.

Second, more detailed information was introduced to the existing pharmacophore model about the substitute on the 5-position of the pyridyl ring. Possibly, the 5-position oriented toward a relative spacious pocket in receptor binding domain and localized in some distance from the wall of the binding domain. Then only a large enough, electronic dense substitute could extend sufficiently to interact with the aromatic amino residue on the wall of the binding domain.

Just as these QSAR models described, in the distance of the 5-position, there were distributed by red contour of electrostatic field (Figure 2), green contour of steric field (Figure 3) and green, yellow color coded at the pyridyl vinyl-substitute (Figure 5). Those suggested preference to rich electron density and certain volume group, and the pyridyl vinyl was one of the most suitable substitutes, whereas in the vicinity of the 5-position, less electronic dense groups of moderate volume would be more suitable.

Finally, for the substitutes of the 6-position of the pyridyl ring, groups were preferred to those with rich electronic density and larger volume. As describe in the HQSAR hologram graphs, the Cl atom was the most suitable group.

Generally, consensus of the three different techniques provided the most efficient way to understand the possible interaction between the ligands and the receptors and furthermore gave significant guidelines for synthesis of novel, potent ligands.

### ACKNOWLEDGMENT

We would like to thank Mr. Hao He and ChemBay Technology Limited Company for providing SGI workstation and related supported software. And we are grateful to Miss Yaling Zhang for her help in the preparation of this manuscript. This work was supported in part by the Research Fund of the Ministry of Education of China for Homecoming Scholars.

### REFERENCES AND NOTES

- (1) Decker M. W.; Brioni J. D.; Bannon A. W.; et al. Diversity of neuronal nicotinic acetylcholine receptors: lesson from behavior and implications for CNS therapeutics. *Life Sci.* **1995**, *56*, 545–570.
- (2) Newhouse, P. A.; Potter, A.; Levin, E. D. Nicotinic systems involvement in Alzheimer's and Parkinson's diseases: Implication for therapeutics. *Drugs Aging* **1997**, *11*, 206–228.
- (3) Lloyd, G. K.; Williams, M. Neuronal nicotinic acetylcholine receptors as novel drug targets. *J. Pharmacol. Exp. Ther.* **2000**, *292*, 461–467.
- (4) Mihailescu, S.; Drucker-Colín, R. Nicotine, brain nicotinic receptors, and neuropsychiatric disorders. *Arch. Medical Res.* **2000**, *31*, 131–144.
- (5) Dani, J. A. Overview of nicotinic receptors and their roles in the central nervous system. *Biol. Psychiatry* **2001**, *49*, 166–174.



- (6) Decker, M. W.; Meyer, M. D.; Sullivan, J. P. The therapeutic potential of nicotinic acetylcholine receptor agonists for pain control. *Expert. Opin. Invest. Drugs* **2001**, *10*, 1819–1830.
- (7) Holladay, M. W.; Dart, M. J.; Lynch, J. K. Neuronal nicotinic acetylcholine receptors as targets for drug discovery. *J. Med. Chem.* **1997**, *40*, 4169–4194.
- (8) Novelloa, R. M.; Gualtieri, F. Cholinergic Nicotinic Receptors: Competitive Ligands, Allosteric Modulators, and Their Potential Applications. *Med. Res. Rev.* **2003**, *23*, 393–426.
- (9) Abreo, M.; Lin, N. H.; Garvey, D.; et al. Novel 3-pyridyl ethers with subnanomolar affinity for central neuronal nicotinic acetylcholine receptors. *J. Med. Chem.* **1996**, *39*, 817–825.
- (10) Lin, N.-H.; Gunn, D. E.; Li, Y.; He, Y.; et al. Synthesis and structure–activity relationships of pyridine-modified analogues of 3-[2-((S)-pyrrolidinyl)methoxy]pyridine, A-84543, a potent nicotinic acetylcholine receptor agonist. *Bioorg. Med. Chem. Lett.* **1998**, *8*, 248–254.
- (11) Lin, N.-H.; Abreo, M. A.; Gunn, D. E.; Lebold, S. A.; et al. Structure–activity studied on a novel series of cholinergic channel activators based on a heteroaryl ether framework. *Bioorg. Med. Chem. Lett.* **1999**, *9*, 2747–2752.
- (12) Lin, N.-H.; Li, Y.; He, Y.; Holladay, M. W.; Kuntzweiler, T.; Anderson, D. J.; Campbell, J. E.; Arneric, S. P. Synthesis and structure–activity relationships of 5-substituted pyridine analogues of 3-[2-((S)-pyrrolidinyl)methoxy]pyridine A-84543: A potent nicotinic receptor ligand. *Bioorg. Med. Chem. Lett.* **2001**, *11*, 631–633.
- (13) Lin, N.-H.; Dong, L.; Bunnelle, W. H.; Anderson, D. J.; Meyer, M. D. Synthesis and biological evaluation of pyridine-modified analogues of 3-(2-Aminoethoxy)pyridine as novel nicotinic receptor ligands. *Bioorg. Med. Chem. Lett.* **2002**, *12*, 3321–3324.
- (14) Lee, J.; Davis, C. B.; Rivero, R. A.; Reitz, A. B.; Shank, R. P. Synthesis and structure–activity relationship of novel pyridyl ethers for the nicotinic acetylcholine receptor. *Bioorg. Med. Chem. Lett.* **2000**, *10*, 1063–1066.
- (15) Brown, L. L.; Kulkarni, S.; Pavlova, O. A.; Koren, A. O.; et al. Synthesis and Evaluation of a Novel Series of 2-Chloro-5-((1-methyl-2-((S)-pyrrolidinyl)methoxy)-3-(2-(4-pyridinyl)vinyl)pyridine Analogues as Potential Positron Emission Tomography Imaging Agents for Nicotinic Acetylcholine Receptors. *J. Med. Chem.* **2002**, *45*, 2841–2849.
- (16) Zhang, Y.; Pavlova, O. A.; Chefer, S. I.; Hall, A. W.; Kurian, V.; et al. 5-Substituted Derivatives of 6-hologeno-3-((2-(S)-azetidiny)methoxy)pyridine and 6-hologeno-3-((2-(S)-pyrrolidinyl)methoxy)pyridine with Low Picomolar Affinity for  $\alpha 4 \beta 2$  Nicotinic Acetylcholine Receptor and Wide Range of Lipophilicity: Potential Probes for Imaging with Positron Emission Tomography. *J. Med. Chem.* **2004**, *47*, 2453–2456.
- (17) Lin, N.-H.; Dong, L.; Bunnelle, W. H.; Anderson, D. J.; Meyer, M. D. Synthesis and biological evaluation of pyridine-modified analogues of 3-(2-Aminoethoxy)pyridine as novel nicotinic receptor ligands. *Bioorg. Med. Chem. Lett.* **2002**, *12*, 3321–3324.
- (18) Schmitt, J. D. Exploring the nature of molecular recognition in nicotinic acetylcholine receptors. *Curr. Med. Chem.* **2000**, *7*, 749–800.
- (19) Tønder, J. E.; Olesen, P. H. Agonists at the  $\alpha 4 \beta 2$  nicotinic acetylcholine receptors: Structure–activity relationships and molecular modelling. *Curr. Med. Chem.* **2001**, *8*, 651–674.
- (20) Tonder, J. E.; Olesen, P.; Hansen, J. B.; Begtrup, M.; Pettersen, I. J. An improved nicotinic pharmacophore and a stereoselective CoMFA-model for nicotinic agonists acting at the central nicotinic acetylcholine receptors labeled by [ $^3\text{H}$ ]-N-methylcarbamylcholine. *J. Comput.-Aided. Mol. Des.* **2001**, *15*, 247–258.
- (21) Nicolotti, O.; Pellegrini-calace, M.; Carrieri, A.; et al. Neuronal nicotinic receptor agonists: a multi-approach development of the pharmacophore. *J. Comput.-Aided. Mol. Des.* **2001**, *15*, 859–872.
- (22) Nicolotti, O.; Pellegrini-Callace, M.; Altomare, C.; Cartotti, A.; Carrieri, A.; Sanz, F. Ligands of Neuronal Acetylcholine Receptor (nAChR): Inferences from the Hansch and 3-D Quantitative Structure–Activity Relationship (QSAR) Models. *Curr. Med. Chem.* **2002**, *9*, 1–29.
- (23) Brejc, K.; van Dijk, W. J.; Klaassen, R. V.; Schuurmans, M.; van der Oost, J.; Smit, A. B.; Sixma, T. K. Crystal structure of an ACh-binding protein reveals the ligand-binding domain of nicotinic receptors. *Nature* **2001**, *411*, 269–276.
- (24) Smit, A. B.; Syed, N. I.; Schaap, D.; van Minnen, J.; Klumperman, J.; Kits, K. S.; Lodder, H.; van der Schors, R. C.; van Elk, R.; Sorgedraeger, B.; Brejc, K.; Sixma, T. K.; Geraerts WPM. A gliaderived acetylcholine-binding protein that modulates synaptic transmission. *Nature* **2001**, *411*, 261–268.
- (25) Schapira, M.; Abagyan, R.; Totrov, M. Structural model of nicotine acetylcholine receptor isotypes bound to acetylcholine and nicotine. *BMC Struct. Biol.* **2002**, *2*, 1–8.
- (26) Le Novère, N.; Grutter, T.; Changeux, J.-P. Models of the extracellular domain of the nicotinic receptors and of agonist- and  $\text{Ca}^{2+}$ -binding sites. *Proc. Natl. Acad. Sci. U.S.A.* **2002**, *99*, 3210–3215.
- (27) Fruchart-Gaillard, C.; Gilquin, B.; Antil-Delbeke, S.; et al. Experimentally based model of a complex between a snake toxin and the  $\alpha 7$  nicotinic receptor. *Proc. Natl. Acad. Sci. U.S.A.* **2002**, *99*, 3216–3221.
- (28) Costa, V.; Nistri, A.; Cavalli, A.; Carloni, P. A structural model of agonist binding to the  $\alpha 3 \beta 4$  neuronal nicotinic receptor. *Br. J. Pharmacol.* **2003**, *140*, 921–931.
- (29) HQSAR is the product of tripos, Inc., St. Louis, MO, 1997.
- (30) Tong, W.; Lowis, D. R.; Perkins, R.; Chen, Y.; Welsh, W. J.; et al. Evaluation of Quantitative Structure–Activity Relationship Methods for Large-Scale Prediction of Chemicals Binding to the Estrogen Receptor. *J. Chem. Inf. Comput. Sci.* **1998**, *38*, 669.
- (31) Huang, X.; Liu, T.; Gu, J.; Luo, X.; Ji, R.; et al. 3D-QSAR Model of Flavonoids Binding at Benzodiazepine Site in GABA<sub>A</sub> Receptors. *J. Med. Chem.* **2001**, *44*, 1883–1891.
- (32) Avery, M. A.; Alvim-Gaston, M.; Woolfrey, J. R. Structure–Activity Relationships of Antimalarial Agent Artemisinin. 6. The Development of Predictive In Vitro Potency Models Using CoMFA and HQSAR Methodologies. *J. Med. Chem.* **2002**, *45*, 292–303.
- (33) Kim, K. H.; Greco, G.; Novellino, A. Critical Review of Recent CoMFA Applications. In *3D QSAR in Drug Design*; Kubinyi, H., Folkers, G., Martin, Y. C., Eds.; Kluwer Academic Publishers: Dordrecht, The Netherlands, 1998; Vol. 3.
- (34) Gohlke, H.; Schwarz, S.; Gundisch, D.; Tilotta, M. C.; Weber, A.; Wegge, T.; Seitz, G. 3D QSAR Analyses-Guided Rational Design of Novel Ligands for the  $(\alpha 4)_2(\beta 2)_3$  Nicotinic Acetylcholine Receptor. *J. Med. Chem.* **2003**, *46*, 2031–2048.
- (35) Zhang, H. B.; Liu, C. P.; Li, H. CoMFA and CoMSIA Studies of nAChRs Ligands: Epibatidine Analogues. *QSAR Comb. Sci.* **2004**, *23*, 80–88.
- (36) Hyperchem 7.0 evaluation release for windows, Hypercube, Inc, 2002.
- (37) Sybyl version 6.91. Tripos Inc., 1699 Hanley Road, St. Louis.
- (38) Ferretti, G.; Dukat, M.; Giannella, M.; Piergentili, A.; et al. Homozanicothine: A Structure-Affinity Study for Nicotinic Acetylcholine (nACh) Receptor Binding. *J. Med. Chem.* **2002**, *45*, 4724–4731.
- (39) Clark, M.; Cramer, R. D., III; Jones, D. M.; Patterson, D. E.; Simeroth, P. E. Comparative molecular field analysis (CoMFA). 2. Toward its use with 3D-structural databases. *Tetrahedron Comput. Methodol.* **1990**, *3*, 47–59.
- (40) Klebe, G.; Abraham, U.; Mietzner, T. Molecular similarity indices in a comparative analysis (CoMSIA) of drug molecules to correlate and predict their biological activity. *J. Med. Chem.* **1994**, *37*, 4130–4136.
- (41) Bush, B. L.; Nachbar, R. B. Sample-distance partial least squares: PLS optimized for many variables, with application to CoMFA. *J. Comput.-Aided Mol. Des.* **1993**, *7*, 587–619.
- (42) Kliebe, G.; Abraham, U.; Mietzner, T. Molecular Similarity Indices in a Comparative Analysis (CoMSIA) of Drug Molecules to Correlate and Predict their Biological activity. *J. Med. Chem.* **1994**, *37*, 4130–4146.
- (43) Toma, L.; Quadrelli, P.; Bunnelle, W. H.; et al. 6-Chloropyridazin-3-yl Derivatives Active as Nicotinic Agents: Synthesis, Binding, and Modeling Studies. *J. Med. Chem.* **2002**, *45*, 4001–4017.

CI0498113